Transient pressure loading of clamped metallic plates with pre-formed holes

K.G. Rakvåg[a,*], N. Underwood[b], G.K. Schleyer[b], T. Børvik[a,c], O.S. Hopperstad[a]

[a] *Structural Impact Laboratory (SIMLab), Centre for Research-based Innovation (CRI) and Department of Structural Engineering, Norwegian University of Science and Technology, Rich. Birkelands vei 1A, NO-7491 Trondheim, Norway*

[b] *University of Liverpool, School of Engineering, Liverpool, L69 3GH, UK*

[c] *Norwegian Defence Estates Agency, Research & Development Department, PB 405, Sentrum, NO-0103 Oslo, Norway*

Abstract

The combined effect of blast and impact loading against protective structures is still not fully understood. In this paper, the motivation is to investigate the combined effect of pressure and fragment loading on steel plates. To simplify the approach, it is assumed that the fragments strike and perforate the flexible target before the pressure load arrives. These perforations are idealized as pre-formed holes of generalized shapes in thin, ductile Docol 600DL steel plates, which are then subjected to controlled pressure pulses in the laboratory. The tests were carried out in a Pulse Pressure Loading Rig, and two different pressure levels were applied for each plate design. After the tests, the deflections caused by the pressure pulses were measured. Even though the plates were much deformed in some of the tests, no sign of failure was observed. Based on a number of material tests, the parameters in the modified Johnson-Cook constitutive relation were identified. Several sets of non-linear finite element simulations of the pressure loading process were then conducted. The agreement between standard Lagrangian simulations and the experimental results was in general good, but the simulations failed to give an accurate description of the deflection around the pre-formed holes. Fully coupled FSI simulations of the experimental tests were then carried out and these simulations demonstrate significant spatial variation of the pressure load. The FSI simulations also showed that this spatial variation of the pressure load influence the deflection profile, especially in the vicinity of the holes.

Keywords: Pressure loading; Docol 600DL steel plates; Experimental tests; FE simulations; FSI simulations.

* Corresponding author: Tel.: +47 73 59 52 02; fax: +47 73 59 47 01.
E-mail address: knut.gaarder.rakvag@ntnu.no (K.G. Rakvåg)

1 Introduction

Design and validation of structures against blast loads are important for modern society in order to protect and secure its citizens. Under such situations the combined effect of blast pressure and fragments impact on structures is assumed to be more severe than the effects of the blast wave or the fragments alone, particularly for close-range external explosions [1][2]. Nevertheless, the standard design methodology today is that these threats are treated independently of each other [3]. This paper is part of a larger research project where the main objective is to investigate the effects of combined blast pressure and fragment impact on thin, ductile steel plates, as virtually all previous works on this problem seem to have been carried out on rigid concrete structures [4][5].

Blast loading or, more general, transient pressure loading of undamaged plates has been studied extensively since World War II, and Nurick et al. [6][7] have compiled reviews of both theoretical and experimental studies on this problem. In later years, the Finite Element Method (FEM) has also been used successfully [8], which makes it possible to accurately describe material properties without simplifications, take non-ideal boundary conditions into account and include stiffeners [9].

Recent advances in FEM also make it possible to investigate the Fluid Structure Interaction (FSI) effects due to large deformations in the plated structure (see e.g. [10] and [11]). Casadei and Potapov [12] published a review of various FSI algorithms for (Arbitrary) Lagrangian-Eulerian analyses. Methods like these allow for analysis of confined explosions in arbitrary geometries such as train carriages inside tunnels [13].

Regarding previous works on plates with holes or other forms of pre-damage, there exist some studies but most of these are not in a general context. Li et al. [14] have investigated the explosion resistance of a square plate with a hole used for venting of dust explosions in the process industry, but few details were given. Langdon et al. [15] have used plates with a hole as a blast mitigation technique, but the interest was not on the behaviour of the plate, but how it altered the blast wave. Schleyer et al. [16] have presented a study on square plates with a central square hole, and both a simplified analytical approach and Lagrangian FE simulations showed no significant reduction in resistance. The motivation for that study was to consider the effect of penetrations in plated deck structures found on offshore topsides and ship bulkheads so as to provide improved limit states assessment criteria to industry on the design of deck

structures under pressure loading. Veldman et al. [17] investigated the response of pre-pressurized plates subjected to blast loading. Their experiments showed that holes from riveted stringers acted as crack initiation locations, due to stress concentrations. They also discussed the possibility that pressure release through the holes results in smaller deflections.

Lightweight and flexible protective structures are increasingly important due to increased use in international operations where mobility is a key factor. In such operations, traditional stationary protective structures made of concrete or similar are of limited utility [18]. Other applications of protective structures, where weight is an important topic, are in design of vehicles, both light vehicles that have to be protected against landmines and improvised explosive devices (IEDs), and VIP vehicles where protection against hand grenades and bullet impacts is important. Mobile and temporary protective structures are important for protection of embassies, government and parliament buildings in limited periods of increased threat. As the use of lightweight ductile materials in protective structures increases, knowledge of the combined effect of pressure loading and fragment impact on these materials is needed. In addition to the relevance for ongoing research on the effect of combined blast and fragment loading, transient pressure loading of plates with holes is relevant for several other applications, such as deck plating on offshore platforms and bulkheads in ships [16], aircraft design [19] and the use of perforated plates for blast wave mitigation [15].

Because tests with cased HE charges induce several uncertainties and much complexity, it is desirable to limit the problem and do experiments in a controlled environment. In this paper, the motivation is to investigate the combined effect of pressure and fragment loading on steel plates. To simplify the approach, it is assumed that the fragments have already hit and perforated the target plate. These perforations are idealized as pre-manufactured holes of generalized shapes in thin, ductile Docol 600DL steel sheets, which are then subjected to controlled pressure pulses in the laboratory. The tests were carried out in a Pulse Pressure Loading Rig, and two different pressure levels were applied for each plate design. Neither the holes in the plate nor the loading generated should be viewed as representative of the case with cased HE charges, but rather as a simplified first approach to a hereto ignored problem, namely the structural response of a plate with holes subjected to pressure loading. Based on tensile tests at a range of strain rates, the parameters of the modified Johnson-Cook constitutive relation were identified. Then, several sets of non-linear finite element simulations of the pressure loading process were conducted using the commercial non-linear finite element code LS-DYNA. First, a set of simulations were carried out in an attempt to reproduce the experimental results and thus to

validate the numerical model. A second set of simulations were used to separate the loading from the plate stiffness, and at last simulations utilizing the FSI capabilities of LS-DYNA were conducted to investigate the loading assumptions and their implications for the deflection of the plate.

2 Experimental setup

2.1 Material

The material used in these experiments is Docol 600DL, a cold-rolled, low-strength and high-hardening steel produced by SSAB in Sweden. Its main use is in the automotive industry, and hence it is delivered in sheets with thickness ranging from 0.5 to 2.1 mm. Gruben et al. [20] have carried out an extensive experimental study on 2 mm thick sheets of Docol 600DL to determine the yield strength, strain hardening and fracture characteristics of the material under quasi-static loading conditions. They also provide material parameters for the strain hardening of the material and showed that the 2 mm thick sheet material is isotropic.

In the pressure loading experiments, sheets of 0.7 mm thickness were used, so additional tensile tests of the 0.7 mm sheet material were carried out in the 0°, 45° and 90° directions with respect to the rolling direction of the plate. Three tests were performed in each direction. These tests were instrumented with an extensometer and the results are thus only valid until diffuse necking. The true stress versus true plastic strain curves from the tension tests are shown in Figure 1 together with results from Gruben et al. [20]. It is seen that the 0.7 and 2 mm thick sheet materials have the same stress-strain behaviour. The differences between the stress-strain curves in the three loading directions are similar to the scatter between repeated tests in each of the directions, and, as a consequence, the material is here considered to be isotropic.

As moderate strain rates are expected in the experiments, the material was tested for strain rate sensitivity in a Split Hopkinson Tension Bar (SHTB). Because the material is only delivered in sheets that are thinner than the thread diameter of our SHTB, a special fixture is needed to connect the specimens with the bars. The specimen is first glued to the fixture, before the threads are milled. The assembly of specimen and fixtures is shown in Figure 2. This experimental setup has been validated by Tarigopula et al. [21]. The 2 mm thick sheet material was tested at five different strain rates ranging from 197 s^{-1} to 879 s^{-1}, since it was practically difficult to test 0.7 mm thick specimens in the SHTB. True stress versus true plastic strain

curves at various strain rates are shown in Figure 3. It is evident that the material is strain-rate sensitive. After the initial transient phase at low strains, the stress-strain curves at high strain rates exhibit additional strain hardening compared with the stress-strain curve at quasi-static strain rate.

The influence of thermal softening on the material has not been investigated in this study. With the expected strains and strain rates in the component tests, adiabatic heating of the material due to plastic dissipation is not expected to have any significant influence on the material behaviour as will be discussed further in Section 4.

2.2 Test rig

The transient pressure loading tests were carried out in the Pulse Pressure Loading Rig (PPLR) at the University of Liverpool. It is capable of producing a repeatable and uniform transient pressure loading over an exposed area of 500×500 mm^2. The test specimen is fixed to the support plate with a clamping plate and 36 bolts. The operating sequence for plates with holes is indicated in Figure 4. First, the chamber is sealed with a rigid plate covering a 500 mm diameter nozzle at one end and a thin film diaphragm covering a 500 mm diameter nozzle at the other. The rig is then pressurized to the desired pressure on each side of the support plate so that no net load is applied to the test plate. At firing, the diaphragm is melted along its circumference by a fuse wire and the air starts to evacuate through the nozzle. The pressure difference is created by the fact that the pressurized air evacuates much quicker through the nozzle than through the holes in the plate.

The side-on pressure is recorded by two pressure transducers at a frequency of 25 kHz, one on each side of the support plate. The location of the pressure transducers on the support plate is shown in Figure 5, together with a test plate mounted with clamping frame and bolts.

As a first approximation, the load on the plate is simplified to be the pressure difference described by the pressure transducers. This simplification is justified by results from experimental tests where additional pressure transducers were used. The additional set of pressure transducers was located close to the centre of the plate, 80 mm away from the closest hole. Figure 6 shows the result from tests with 15, 25 and 50 psi pressures. It is evident that there is little variation between the pressure recorded on the test specimen and the pressure recorded at the original location on the support plate.

2.3 Plates

Four different plate designs with pre-formed holes, as shown in Figure 7, were tested. The geometries of the holes (i.e. square holes, diamond-shaped holes, circular holes and slits) were chosen to represent idealized holes in the plate made by perforating fragments. It was decided to distribute the holes across the plates so that the area of the holes varies while the minimum distance between the holes is constant and equal to 100 mm, as shown in Figure 7.

The outer dimensions for each plate are 660×660 mm^2, while the area exposed to the pressure-load is 500×500 mm^2 minus the area of the holes. Each plate has a nominal thickness of 0.7 mm, so plastic membrane stretching is assumed to be the primary mode of deformation. The area of the holes and the area exposed to the pressure load for each plate are summarized in Table 1. Each plate design is tested at two nominal gauge pressures: 172 kPa and 345 kPa, corresponding to 25 psi and 50 psi, respectively.

3 Experimental results

3.1 Pressure-time curves

Recorded pressure-time curves for each experiment are shown in Figure 8. The pressure load varies considerably with the plate design. Both the maximum pressure and the duration (and consequently also the impulse defined as the integral of the load with respect to time) increase with decreasing hole area, as expected due to the confinement of the test rig. Measured maximum pressure, duration and impulse from each test are given in Table 2. The impulse to the plate is increased by a factor of more than five when the pre-formed holes in the plate are changed from squares to slits. Unfortunately, the pressure recording for the plate test with slits at 25 psi nominal pressure did not record properly, and is therefore not presented. It should be noted that with the geometrical limitations of the experimental setup, the differences between the pressure-time curves for the various plate designs are more pronounced than the differences in reflected pressure would have been for the same plates in a free-field explosion.

3.2 Deflections

The permanent midpoint deflections of the tested plates are summarized in Table 3 and Figure 9 as a function of the area of the holes. An interesting observation is that no monotonic relation exists between the measured permanent deflection and the area of the holes. However, the

general trend is that the final deflection increases as the area of the holes decreases. This can be attributed to the increase in pressure and impulse with decreasing hole area. The increased pressure also acts on a larger surface as the area of the holes decreases, which further amplifies the load transmitted to the plate. Thus, the decrease in stiffness associated with the increasing area of the holes is more than compensated for by the decrease in the load.

The increase in the permanent midpoint deflection of the plate when going from a square hole to a slit is only a fraction of the corresponding increase in transferred impulse (see Table 2 and Table 3). This suggests that the load cannot be classified as impulsive loading and, consequently, the complete pressure-time history is needed for each situation.

Another observation is that the plates with circular holes do not fit this pattern, indicating that not only the size of the holes influences the stiffness, but also the shape of the holes. The results show the complex effect that discontinuities have on the deflection of the plates. Deformed shapes of the various plates after the 25 psi series of loading are shown in Figure 10. Visual inspection of the plates identified plastic hinges at the edges, but no plastic hinges within the plates, except for a few centimetres towards the corners. Thus, the primary load bearing mode of the plates is membrane stretching. Because both the plate stiffness and the load level vary, it is difficult to make strict conclusions from the experiments alone, but they can be used to validate numerical methods which in turn can be used for further studies. Deflection profiles along several sections of the plates were also measured after each test. The measured displacement fields will be discussed and compared against the numerical results in the next section.

4 Numerical simulations

Several sets of numerical simulations of the pressure-loaded plates have been performed in this study. Firstly, numerical simulations of the experimental tests using a Lagrangian solver were conducted to validate the numerical model. Secondly, a parametric study was carried out to investigate how the pre-formed holes altered the response of the plate. Finally, fully coupled Lagrangian-Eulerian simulations were performed to investigate if it can be justified to neglect fluid-structure interaction effects. Quarter-symmetric boundary conditions were utilized in all simulations to save computational time.

4.1 Constitutive relation

All simulations were run in LS-DYNA version 971 [22][23]. The plates were modelled using under-integrated Belytschko-Tsay shell elements and the material was described using the modified Johnson-Cook constitutive relation [24]. The von Mises equivalent stress $\bar{\sigma}$ in the modified Johnson-Cook constitutive relation, including the extended Voce hardening rule, is expressed as

$$\bar{\sigma} = \left[A + \sum_{i=1}^{2} Q_i \left(1 - \exp\left(-C_i \bar{\varepsilon}\right)\right) \right] \left[1 + \frac{\dot{\bar{\varepsilon}}}{\dot{\bar{\varepsilon}}_0} \right]^c \left[1 - \left(\frac{T - T_r}{T_m - T_r} \right)^m \right] \tag{1}$$

where $\bar{\varepsilon}$ is the equivalent plastic strain, $\dot{\bar{\varepsilon}}$ is the equivalent plastic strain rate and $\dot{\bar{\varepsilon}}_0$ is a user-defined reference strain rate. The constant A determines the initial yield strength of the material, whereas Q_i and C_i, $i = 1, 2$, define the strain hardening. The rate sensitivity is governed by the constant c, while m defines the thermal softening behaviour. The homologous temperature is defined as $T^* = \left(T - T_r\right) / \left(T_m - T_r\right)$, where T is the absolute temperature, T_r is the ambient temperature and T_m is the melting temperature. The temperature change due to adiabatic heating may be calculated as

$$\Delta T = \int_0^{\bar{\varepsilon}} \chi \frac{\bar{\sigma} d\bar{\varepsilon}}{\rho C_p} \tag{2}$$

where ρ is the material density, C_p is the specific heat and χ is the Taylor-Quinney coefficient that represents the proportion of plastic work converted into heat.

The yield strength and strain hardening parameters presented in Table 4 are taken from Gruben et al. [20]. Owing to the increased strain hardening of the material at high strain rates, the modified Johnson-Cook constitutive relation is not capable of accurately capturing the rate sensitivity at different levels of plastic strain. Figure 11 shows the flow stress as a function of the logarithmic strain rate for three different levels of plastic strain. It is seen that different values of c are needed to fit the experimental data when the plastic strain increases, while the reference strain rate $\dot{\bar{\varepsilon}}_0$ is constant and equal to 33 s^{-1}. Note that the result from the test at strain rate 879 s^{-1} is not included in Figure 11 due to uncertainties in the measurements (see Figure 3).

Since the plastic strains in the pressure-loaded plates are rather small and the strain rates below the conditions for adiabatic heating, thermal softening is not assumed to influence the behaviour of the material. The simulations confirmed that the maximum equivalent plastic strain was about 3 % and that the maximum strain rate was 10 s^{-1}. A sensitivity study showed that the predicted response was affected neither by the moderate rate sensitivity of the material nor by thermal softening. Accordingly, the parameters c and m are henceforth set to their default values 0 and 1, respectively, which implies that rate sensitivity is neglected and a linear decrease of the flow stress with increasing temperature is assumed in the simulations.

4.2 Lagrangian simulations

The finite element mesh used for the plates with square holes is shown in Figure 12. Visual inspection of the plates after the tests showed that there was severe straining around the bolts. This was not surprising considering that the plates were very thin and thus have to carry the load through membrane forces. Because of this it was found important to model the boundary conditions with a sufficient degree of accuracy to capture this straining. Preliminary simulations showed that it was necessary to include the bolts in the finite element model, and they were modelled with analytical rigid walls in LS-DYNA. Initial stresses that could arise in the vicinity of the holes from the cutting process are neglected in this study. A sensitivity study on the influence of the mesh density was also carried out, and the details of this study are shown in Table 5. Element sizes between 16×16 mm^2 and 2×2 mm^2 were used. The results showed that the mesh-size sensitivity of the problem is minor, and that a mesh size of 4×4 mm^2 seems to be sufficient to obtain a converged solution. In the simulations, the recorded pressure-time curves from the experiments were applied to the respective plate designs. As seen from Table 6 and Figure 13, the numerical simulations are capable of reproducing the experimental permanent midpoint deflections with reasonable accuracy. The two major exceptions are the 50 psi test on the plate with slits and the 25 psi test of the plate with circular holes.

To have a better basis of comparison, the tested plates were also profiled manually by using a grid aligned with the bolt holes, and then the measured displacement fields were compared to those obtained in the numerical simulations. This way it was possible to check to what extent the overall deformation pattern was correctly predicted, not only the midpoint deflection. Figure 14 to Figure 17 show some of the measured experimental profiles compared with corresponding profiles from the numerical simulations. Because the problem is assumed quarter-symmetric and this symmetry was used in the finite element model, the average values from the

experimental profiles are plotted. In addition, the minimum and maximum measurements for each quarter-symmetric point are plotted as error bars. Figure 14 shows that the numerical simulations are capable of reproducing the experimental deflections for plates with square holes in a satisfactory manner, except in the vicinity of the holes. Close to the holes the simulations do not capture the experimental deflections in either shape or size. This is illustrated in Figure 15, which shows that none of the simulations are capable of capturing accurately the bulging pattern observed along the lines shown in the figure.

The same observations are made for the plates with diamond-shaped holes, as shown in Figure 16 and 17. The profiles away from the holes match the experimental results quite accurately. Close to the holes the deviations between experimental and numerical results are much larger. Profiles are only shown for the plates with square and diamond-shaped holes, because these are the plate designs where the midpoint deflections were reproduced for both the 25 psi and 50 psi tests. Mesh refinements from a characteristic element length of 8 mm to 2 mm did not give any better results. The reason for the discrepancies is assumed to be that the local loading close to the holes in the plates is not properly described with the simplified approach used in this section. The loading will be further examined in Section 4.3.

Finally, the predicted deformed shapes close to the holes of the various plates are plotted in Figure 18. The fringes represent the equivalent plastic strain field. Even though the deflections of the various plates are in the order of 20 times the plate thickness, the plastic strains are small. The fringe levels in Figure 18 have a maximum of 3% plastic strain, and it is seen that this level is only exceeded locally. The plastic hinges at the edges are well reproduced in the simulations, while the plastic hinges towards the corners of the plates, as indicated in Figure 10, are not captured in the numerical analyses. The comparison of the plastic strains in the different plate designs reveals that there is a band of plastic strain in the minimum cross-section between the holes. The width of the band and the magnitude of plastic strain within it are similar for the different plates. However, the location and size of the area with maximum plastic strain depend markedly on the plate design.

To study how the holes alter the stiffness of the plates, two additional series of numerical simulations were performed. In these simulations, the same pressure-time history was applied to all plate designs. The pressure-time histories from the 25 psi square holes test and the 50 psi diamond-shaped holes test were adopted in the simulations. In the first series of simulations, the pressure was applied to the entire exposed area of each plate design, which implies that even

though the pressure-time history was the same for all plates, the total load transmitted to the plate still varied with the area of the holes. In the second series of simulation, the pressure was applied to an area of the plate which corresponds to the exposed area of the plate with square holes, and thus only the stiffness of the plate varied between the different simulations. Figure 19 shows the results from the first series of simulations in terms of permanent deflection as a function of the area of the holes. It is seen that when equal pressure-time histories are applied to the different plate designs, the permanent midpoint deflection is approximately constant. It is concluded that the reduction in stiffness due to the holes is compensated by the reduced area to which the load is applied. The results from the second series of simulations are presented in Figure 20. From this plot it is clear that when the same pressure-time history is applied to an equal area for all the plate designs, the intuitive result that the permanent deflection increases when the area of the holes increases is obtained.

These simulations emphasize that the effect of introducing holes in a plate exposed to transient pressure loading is dependent on the loading conditions. If the load is confined, as in these experiments, the effect is that the displacement decreases with increasing hole size, because of the less constrained flow through the holes. In a free-field explosion, where the overpressure is free to flow around the structure, the holes will probably reduce the load to a less extent and the trend will be more like the results in Figure 19.

4.3 Fluid Structure Interaction simulations

To investigate the spatial variation of the pressure loading, the FSI capabilities of LS-DYNA were utilized. A simplified numerical model of the test rig with a plate with square holes is shown in Figure 21. Quarter-symmetry boundary conditions are used. The test rig is modelled as a rectangular box with a length of 1 m, i.e. the same length as the actual test rig. The depth and width are 0.37 m, such that the total volume is equal to the volume of the actual test rig. The walls of the rig are modelled as fixed boundary conditions, except for the nozzle outlet where the air is allowed to flow out of the model and into an ambient domain with initial atmospheric pressure. In the experiments, the nominal diameter of the outlet is 0.5 m, but the fuse wire that melts the diaphragm covering the outlet is not in direct contact with the steel boundary. This is done to avoid short-circuiting of the current, and reduces the effective diameter of the nozzle output. The outlet diameter is thus modelled as 0.46 m in the FSI simulations.

The plate is still modelled with shell elements using reduced integration and hourglass control, while the pressurized air is modelled with $10\times10\times10$ mm^3 under-integrated ALE multi-material solid elements using the gamma law equation of state [23] given as

$$P = (\gamma - 1)\left(\frac{\rho}{\rho_0}E\right) \tag{3}$$

Equation (3) gives the pressure P of a perfect gas as a function of the heat capacity ratio γ, the current density ρ, the reference density ρ_0 and the initial internal energy per unit reference volume E. The values for air at 0 and 25 psi gauge pressure are given in Table 7 [25]. The fluid-structure interaction (FSI) between the rigid plate and the air is modelled using a penalty based coupling between the Lagrangian solid and the Eulerian fluid.

The permanent midpoint deflections from the FSI simulations are compared with both the experimental values and the corresponding results from the simplified Lagrangian simulations in Figure 22. The displacements compare well with the simplified Lagrangian results, also for the plate with circular hole which did not compare well with the experimental results. However, the result from the FSI simulation for the plate with slits show a good agreement with the experimental value. Note that the CPU-time increased from typically 1 hour for a Lagrangian simulation of the problem to more than 14 hours for a similar FSI simulation. For the pressure recordings, several comparisons are carried out.

First, the pressure-time histories are calculated from an analysis in the same way as in the experiments, i.e. the side-on pressure of the air is recorded at the locations of the pressure transducers in the experiments, and the pressure load is taken as the difference in pressure between these two points on each side of the plate. These pressure-time histories from the FSI simulations are compared with the experimentally obtained histories in Figure 23, where it is seen that the simulated pressure-time histories have a peak value that is around 10% lower than the experimental value. Apart from that the predicted and experimental curves are in good agreement, and the trend of higher pressure as a function of smaller hole is predicted.

Second, the actual load transmitted to the plate by the penalty contact is calculated, both for the complete plate and for the band of elements that are closest to the hole (i.e. the band of green elements indicated in Figure 21). These two curves are plotted in Figure 24 together with the predicted pressure difference curves. It is seen that the pressure difference is a very good

approximation for the average pressure on the plate, as the two curves are virtually on top of each other. However, it is also evident that the pressure load on the elements closest to the hole is about 50 % higher than the average pressure load on the plate. This numerical result offers a possible explanation for the discrepancies in deflection profile presented in Figure 15 and Figure 17; namely that there seems to be an FSI effect which increases the pressure load in the proximity of the holes. This effect could explain the increased local deflection around the holes in the plates.

At last, plates with holes of the same area are simulated. The plate with square holes is used as a reference, and the plates with circular and diamond holes are modified with larger holes such that the area of the holes are now equal. The fluid mesh is the same as in the previous simulations, and the initial gauge pressure is 25 psi. The results are summarized in Table 8 where it is seen that the maximum of the average load on the plate is more or less equal, since the area of the holes are now the same. The permanent midpoint deflections from the FSI simulations corroborate the observation from experiments that the shape of the hole is important. The plate with circular holes has no significant increase in permanent midpoint deflection compared to the plate with square holes, while the plate with diamond holes has a significant increase in permanent midpoint deflection compared with the two other plates. To demonstrate the influence of local FSI effects such as a spatial variation of the pressure load, a set of Lagrangian simulations of the plates with holes of the same area was carried out. The predicted average pressure on the plate from the FSI simulations are used as load curves in the Lagrangian simulations, implying that any difference between the two sets of simulations is due to spatial variation of the pressure load. The permanent midpoint deflections from the Lagrangian simulations are shown together with the FSI results in Table 8. The difference in permanent midpoint deflection is not considerable, but a comparison of the deflection profiles show that the local effects are more prominent. In Figure 25 the permanent deflection profiles for the plate with square holes along the directed lines used in Figures 14 and 15 are shown for both the FSI and the Lagrangian simulations. Here it is seen that the difference between the two cases are most prominent around the holes, which is not surprising given the significant increase in pressure around the hole demonstrated in Figure 24.

5 Discussion and conclusions

The experiments and numerical simulations presented above show that modest alterations to the geometry of a pressure-loaded structure in the form of holes do not seem to degrade the structural resistance when the impulse is sufficiently low not to cause the plate to fail, at least not for very ductile materials like the one used in this study. The decrease in stiffness caused by the pre-formed holes is compensated by a reduced load area and hence pressure load. The experimental results also show that even though the plates were markedly deformed in some of the tests, there was no sign of failure between the holes. However, the damage introduced to a plate by fragment perforation will leave behind holes with rougher edges and sharper cracks than the pre-formed holes applied in this study.

As also observed both in the experiments and numerical simulations, the smallest deflection was found for the plates with circular holes independent of pressure loading. Thus, it is not only the size of the holes that is important, but also the shape. The shape of the holes would be even more important if the plates were loaded to fracture, because crack initiation is highly dependent on the stress state, which varies with the shape of the hole [26].

The comparison of deflection profiles from experiments and numerical simulations discloses the important effect of simplifying the transient pressure load as uniform over the exposed area of the pre-damaged plates, namely that the simulations under-estimate the deflections in the vicinity of the holes. It stands to reason that the fluid flow through the holes alters the loading in their neighbourhood. Wadley et al. [27] have shown that FSI effects due to local deformations only show up in the numerical analyses when the load is properly described. They also concluded that on a global scale, the FSI effects are not so important, but they are needed to describe the behaviour at the local scale. Even though the results from Wadley et al. [27] are from a different problem, they support the explanation that the discrepancies between the predicted and experimentally-obtained plate deflections in the area close to the holes are the result of a spatial variation of the pressure load.

The FSI simulations performed in this study also supports this explanation. The simulations show that the side-on pressure difference between the two chambers is a good approximation of the average pressure on the exposed area. However, the FSI simulations also show that there is a region of higher pressure in the vicinity of the holes, and the deflection profile from the FSI simulation is different than the profile obtained from the Lagrangian simulation with uniform

pressure load. The Lagrangian simulations with the simplified load description are capable of reproducing the global deflection pattern, but fail to capture the increased deflection around the holes due to the FSI effect. The FSI simulations also show that the region of higher pressure is confined to a narrow band around the holes, which explains why the higher pressure is not evident in the experimental results shown in Figure 6.

From the Lagrangian simulations in which the applied pressure-time history is the same for all tests, it is seen that the maximum deflection is more or less the same for all plate designs. As this probably is the loading condition closest to a free-field explosion, where the blast wave can escape around the structure and thus the mitigation effect of holes in the plate is reduced, the generality of this observation should be examined in further work. In this study, the holes were designed with different areas so that the minimum distance between the holes was equal. FSI simulations of plates with holes of equal area, such that the applied pressure and loaded area are approximately equal for the different plate designs, show the importance of the shape of the hole.

It should finally be noted that for these results to be valid for a combined blast and fragment loading case, the stand-off distance must be large enough for the fragments to reach the plate before the blast wave, and that the fragments must perforate the structure. If the fragments do not perforate the plate or the blast wave reaches the plate before or simultaneously as the fragments, the total load will be equal to the sum of the contributions from the blast wave and the fragment impact [28].

Acknowledgement

The financial support of this work from the Structural Impact Laboratory (SIMLab), Centre for Research-based Innovation (CRI) at the Norwegian University of Science and Technology (NTNU), is gratefully acknowledged.

References

[1] Leppänen J. Experiments and numerical analyses of blast and fragment impacts on concrete. International Journal of Impact Engineering 2005;31:843-860.

[2] Baker WE, Cox PA, Westine PS, Kulesz JJ, Strehlow RA. Explosion hazards and evaluation. Amsterdam: Elsevier Scientific Publishing Company, 1983.

[3] U.S. Army Engineers Waterways Experiment Station. TM 5-855-1 – Fundamentals of protective Design for Conventional Weapons, 1991.

[4] Nyström U, Gylltoft K. Numerical studies of the combined effects of blast and fragment loading. International Journal of Impact Engineering 2009;36:995-1005.

[5] Hu W and Chen Z. Model-based simulation of the synergistic effects of blast and fragmentation on a concrete wall using the MPM. International Journal of Impact Engineering 2006;32:2066-2096.

[6] Nurick GN, Martin JB. Deformations of thin plates subjected to impulsive loading—a review; Part I—theoretical consideration. International Journal of Impact Engineering 1989;18:159-170.

[7] G Nurick GN, Martin JB. Deformations of thin plates subjected to impulsive loading—a review; Part II—experimental studies. International Journal of Impact Engineering 1989;18:170-186.

[8] Belytschko T, Marchertas AH. Nonlinear Finite-Element Method for Plates and Its Application to Dynamic Response of Reactor Fuel Subassemblies. Journal of Pressure Vessel Technology 1974;96:251-257.

[9] Langdon GS, Schleyer GK. Deformation and failure of profiled stainless steel blast wall panels. Part III: finite element simulations and overall summary. International Journal of Impact Engineering 2006;32:988-1012.

[10] Børvik T, Hanssen AG, Langseth M, Olovsson L. Response of structures to planar blast loads – A finite element engineering approach. Computers & Structures 2009;87:507-520.

[11] Børvik T, Olovsson L, Hanssen AG, Dharmasena KP, Hansson H, Wadley HNG. A discrete particle approach to simulate the combined effect of blast and sand impact loading of steel plates. Journal of the Mechanics and Physics of Solids 2011;59:940-958.

[12] Casadei F, Potapov S. Permanent fluid–structure interaction with non-conforming interfaces in fast transient dynamics. Computer Methods in Applied Mechanics and Engineering 2004;193:4157–4194

[13] Larcher M, Casadei F., Solomos G. Risk analysis of explosions in trains by fluid–structure calculations. Journal of Transportation Security 2010;3: 57-71.

[14] Li G, Chen B-Z, Deng X-F, Eckhoff RK. Explosion resistance of a square plate with a square hole. Journal de Physique IV 2002;12:121-124.

[15] Langdon GS, Rossiter IB, Balden VH, Nurick GN. Performance of mild steel perforated plates as a blast wave mitigation technique: Experimental and numerical investigation. International Journal of Impact Engineering 2010;37:1021-1036.

[16] Schleyer GK, Underwood N, Do HM, Paik JK, Kim BJ. On the simplified analysis of square plates with holes. Proceedings of the ASME 2011 30th International Conference on Ocean, Offshore and Arctic Engineering. ASME, Rotterdam, pp 1-5.

[17] Veldman RL, Ari-Gur J, Clum C. Response of pre-pressurized reinforced plates under blast loading. International Journal of Impact Engineering 2008;35:240-250.

[18] Børvik T, Hanssen AG, Dey S, Langberg H, Langseth M. On the ballistic and blast load response of a 20 ft ISO container protected with aluminium panels filled with a local mass — Phase I: Design of protective system. Engineering Structures 2008;30:1605-1620.

[19] Simmons MC, Schleyer GK. Pulse pressure loading of aircraft structural panels. Thin-Walled Structures 2006;44:496-506.

[20] Gruben G, Fagerholt E, Hopperstad OS, Børvik T. Fracture characteristics of a cold-rolled dual-phase steel. European Journal of Mechanics - A/Solids 2011;30:204-218.

[21] Tarigopula V, Hopperstad OS, Langseth M, Clausen AH, Hild F. A study of localisation in dual-phase high-strength steels under dynamic loading using digital image correlation and FE analysis. International Journal of Solids and Structures 2008;45:601-619.

[22] LS-DYNA, LS-DYNA Theory Manual, Livermore Software Technology Corporation (2006), V. 971.

[23] LS-DYNA, LS-DYNA Keyword User's Manual, Livermore Software Technology Corporation (2007), V. 971.

[24] Børvik T, Hopperstad OS, Berstad T, Langseth M. A computational model of viscoplasticity and ductile damage for impact and penetration. European Journal of Mechanics - A/Solids 2001;20:685-712.

[25] Mullin MJ, O'Toole BJ. Simulation of energy absorbing materials in blast loaded structures. In: Proceedings of eighth international LS-DYNA users conference, May 2–4, 2004

[26] Anderson TL, Fracture mechanics, Taylor & Francis, 2005.

[27] Wadley HNG, Børvik T, Olovsson L, Wetzel JJ, Dharmasena KP, Hopperstad OS, Deshpande VS, Hutchinson J. Deformation and fracture of impulsively loaded sandwich panels. Submitted for possible journal publication, 2012.

[28] Krauthammer T. Investigation of structurally composite panels for protective systems. SIMLab workshop on modeling and behaviour of light-weight protective structures, Trondheim, Norway, 2-3 December 2010.

Table 1: Plate designs.

	Square	Circle	Diamond	Slit
Hole Area [m^2]	0.04	0.0314	0.02	0.0032
Exposed Area [m^2]	0.21	0.2186	0.23	0.2468
Exposed Area [%]	84	87.4	92	98.7

Table 2: Measured maximum pressure, duration and impulse from each test.

	Maximum pressure [kPa]		Duration [s]		Specific Impulse [kPa s]	
Nominal test pressure	172 kPa (25 psi)	345 kPa (50 psi)	172 kPa (25 psi)	345 kPa (50 psi)	172 kPa (25 psi)	345 kPa (50 psi)
Square	132	230	0.051	0.069	2.7	6.5
Circle	143	245	0.064	0.073	3.3	7.4
Diamond	152	283	0.108	0.128	5.4	13.2
Slit	-	312	-	0.367	-	32.9

Table 3: Measured permanent midpoint deflections.

Nominal Test Pressure	Square [mm]	Circle [mm]	Diamond [mm]	Slit [mm]
172 kPa (25 psi)	16.8	9.35	18.2	22.5
345 kPa (50 psi)	20.7	17.2	22.8	31.2

Table 4: Yield stress and strain hardening constants for Docol 600DL steel [20].

A [MPa]	Q_1 [MPa]	C_1	Q_2 [MPa]	C_2
283	268	39.4	396	5

Table 5: Details of mesh convergence study on plate with square holes and 50 psi nominal test pressure

Characteristic element size [mm^2]	16x16	8x8	8x8 (SRI)*	4x4	2x2
Midpoint deflection [mm]	20.75	21.49	21.28	22.66	23.02
Max deflection at perimeter of hole [mm]	20.36	21.02	20.77	22.23	22.62
Hourglass energy as % of internal energy [%]	3	1.3	0	0.8	0.4
Run time [s]	93	658	1544	4129	37713

* SRI = Selective reduced integration

Table 6: Predicted midpoint deflections obtained from Lagrangian simulations.

Nominal Test Pressure	Square [mm]	Circle [mm]	Diamond [mm]	Slit [mm]
172 kPa (25 psi)	17.2	16.7	18.9	-
345 kPa (50 psi)	22.7	21.7	24.4	27.2

Table 7: Parameters for the gamma law of air at 0 and 25 psi gauge pressure [25].

Gauge pressure	ρ_0 [kg/m^3]	γ	E [kJ/kg]
0 psi	1.27	1.4	250
25 psi	3.46	1.4	681

Table 8: Results from FSI simulations on plates with holes of the same area

	Square	Circle	Diamond
Max pressure load [kPA]	107	108	105
Permanent midpoint deflection FSI [mm]	18.1	18.3	21.2
Permanent midpoint deflection Lagrangian [mm]	17.6	18.1	20.2

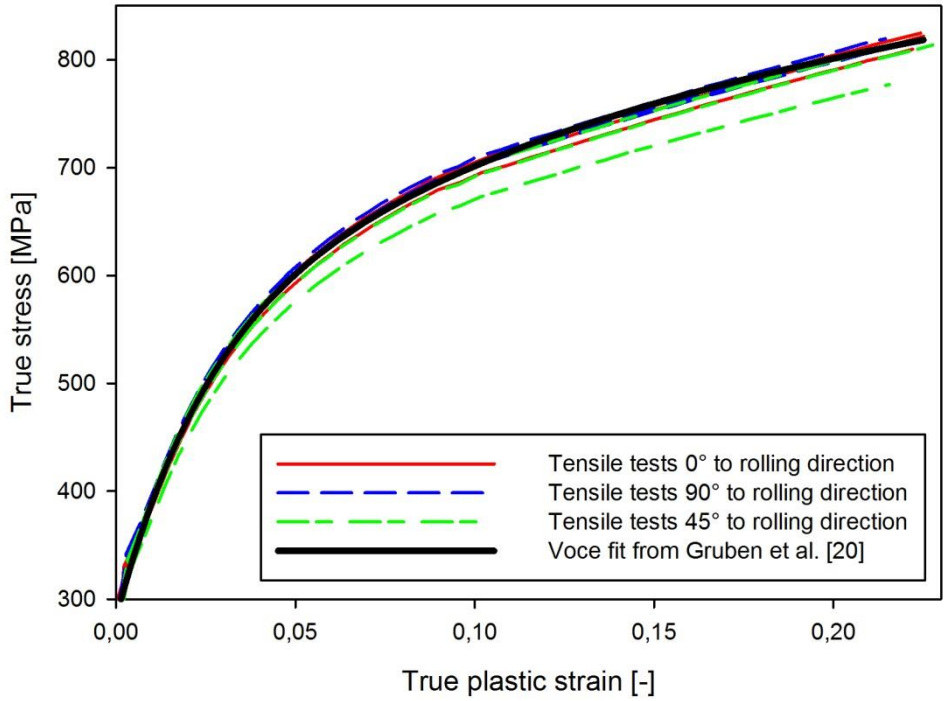

Figure 1: True stress versus true plastic strain curves in uniaxial tension at $0°, 45°$ and $90°$ directions with respect to the rolling direction for the 0.7 mm thick Docol 600DL steel sheet.

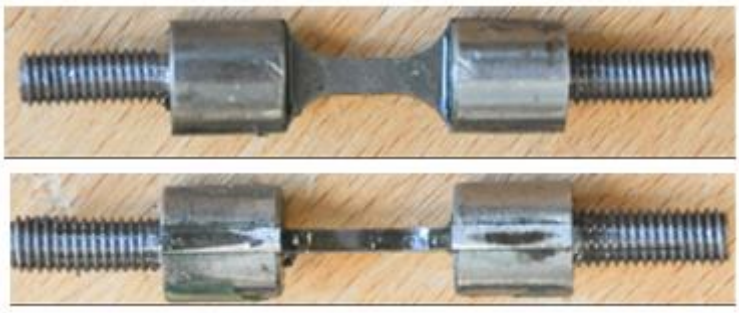

Figure 2: Assembly of specimen and fixture for tension testing of thin sheets at high-strain rates.

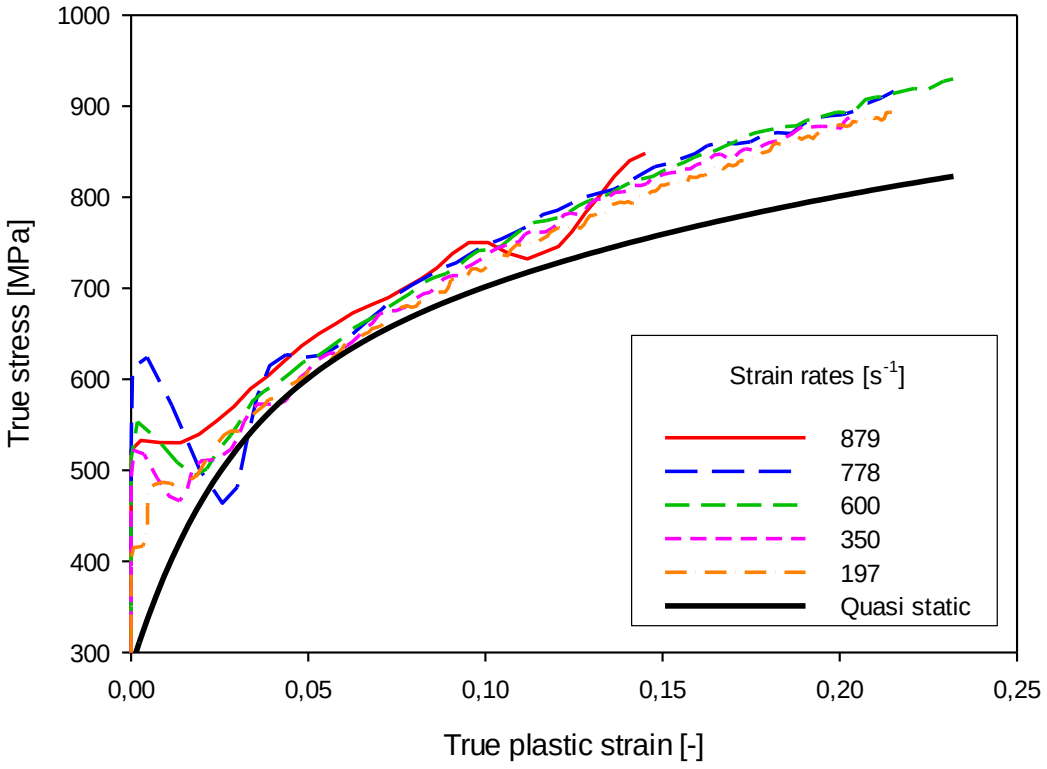

Figure 3: True stress versus true plastic strain curves at various strain rates for a 2 mm thick Docol 600DL sheet.

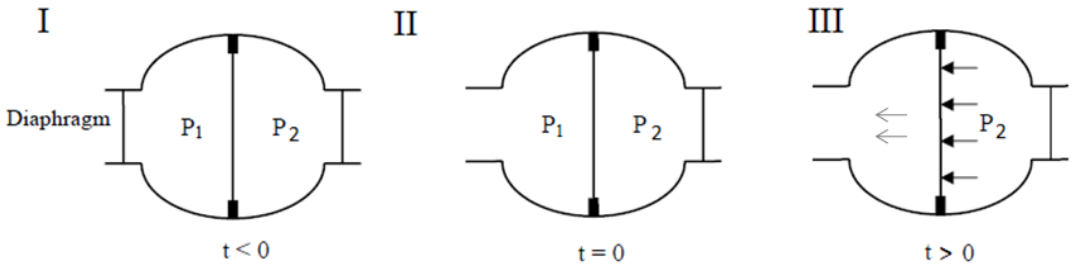

Figure 4: Schematic illustration of the operating sequence of the rig for plates with holes. I: Both sides of the test specimen are pressurized to the desired nominal pressure. No net load is acting on the plate (i.e. $P_1 = P_2$), since the holes in the test specimen equalize the pressure. II: The diaphragm is melted along its circumference, and the nozzle outlet is open so that $P_1 < P_2$.

III: A net load is created on the test specimen because the pressurized air evacuates quicker through the nozzle outlet than through the holes in the test specimen.

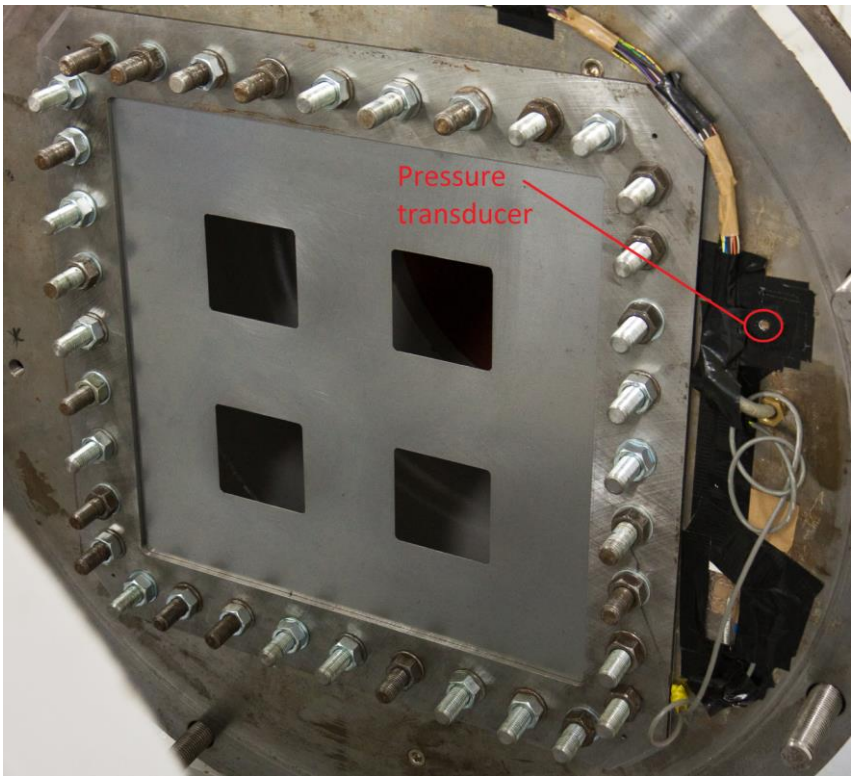

Figure 5: The test rig's support plate and the test specimen which is mounted with 36 bolts. The location of the pressure transducer is indicated in the figure.

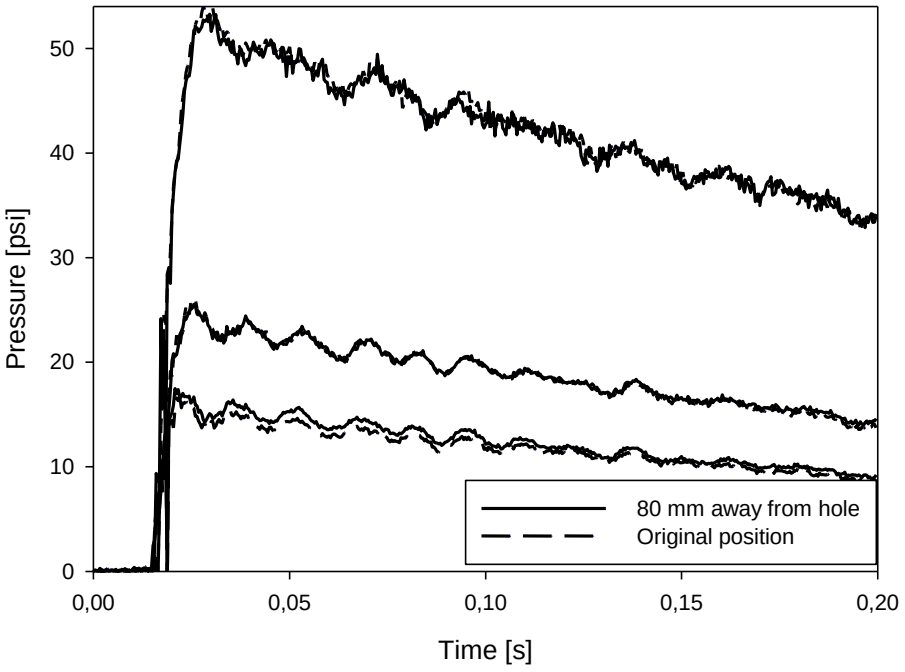

Figure 6: Comparison of pressure-time measurements at original position and 80 mm away from the closest hole for three different pressure levels.

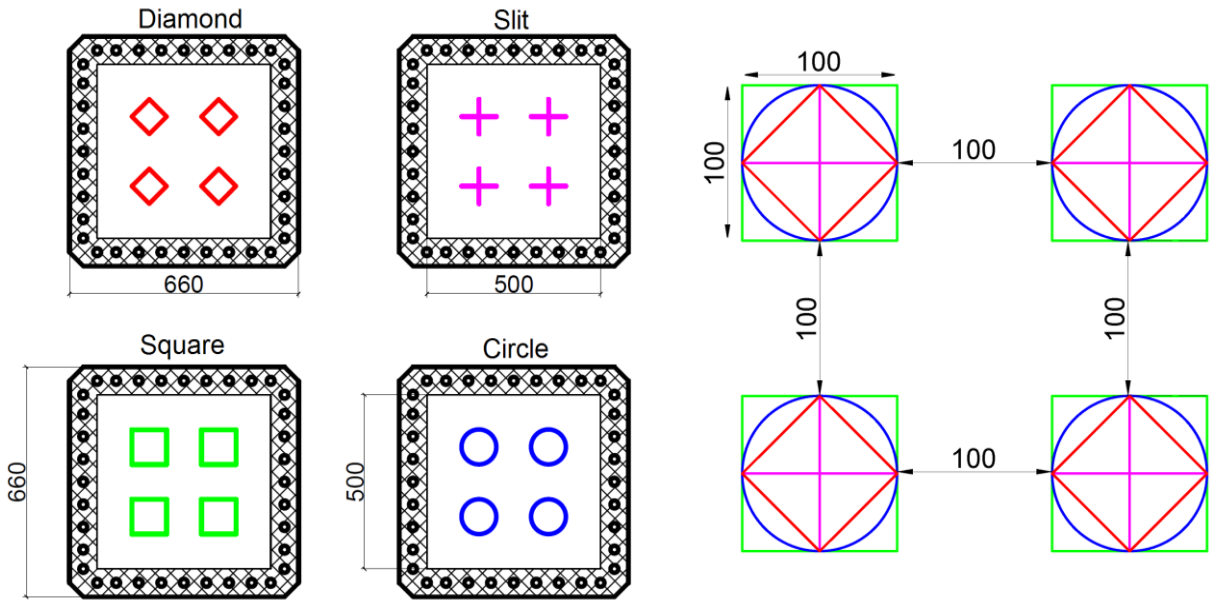

Figure 7: The four different plate designs used in the study are shown to the left. To the right, the four different plate designs are superimposed to show that the minimum distance between the holes is equal in all cases. All measures are in mm.

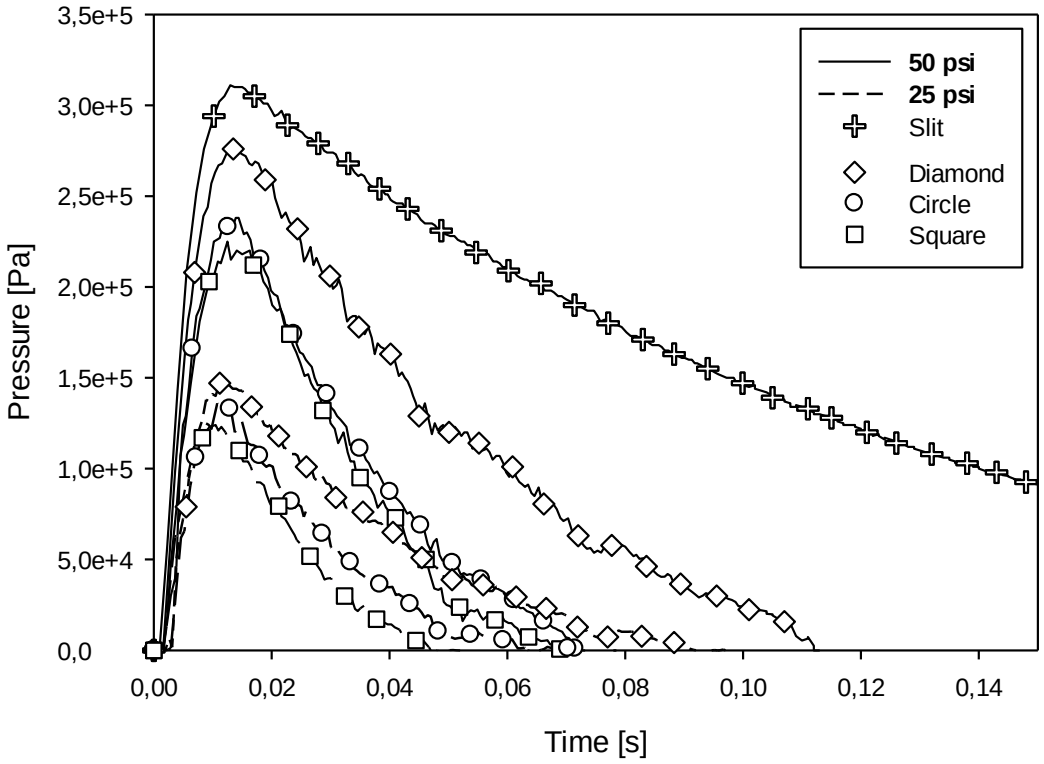

Figure 8: Recorded pressure-time curves from the experiments.

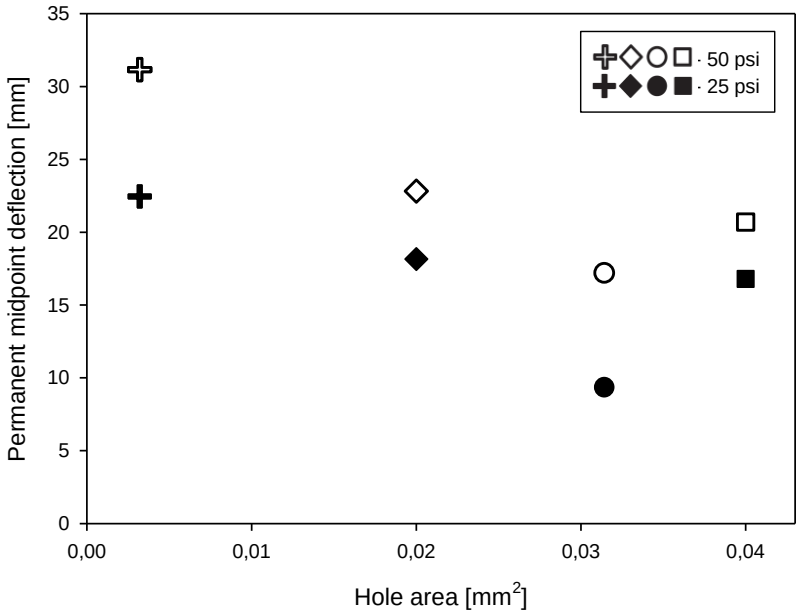

Figure 9: Permanent midpoint deflections measured from experiments shown as a function of increasing hole area.

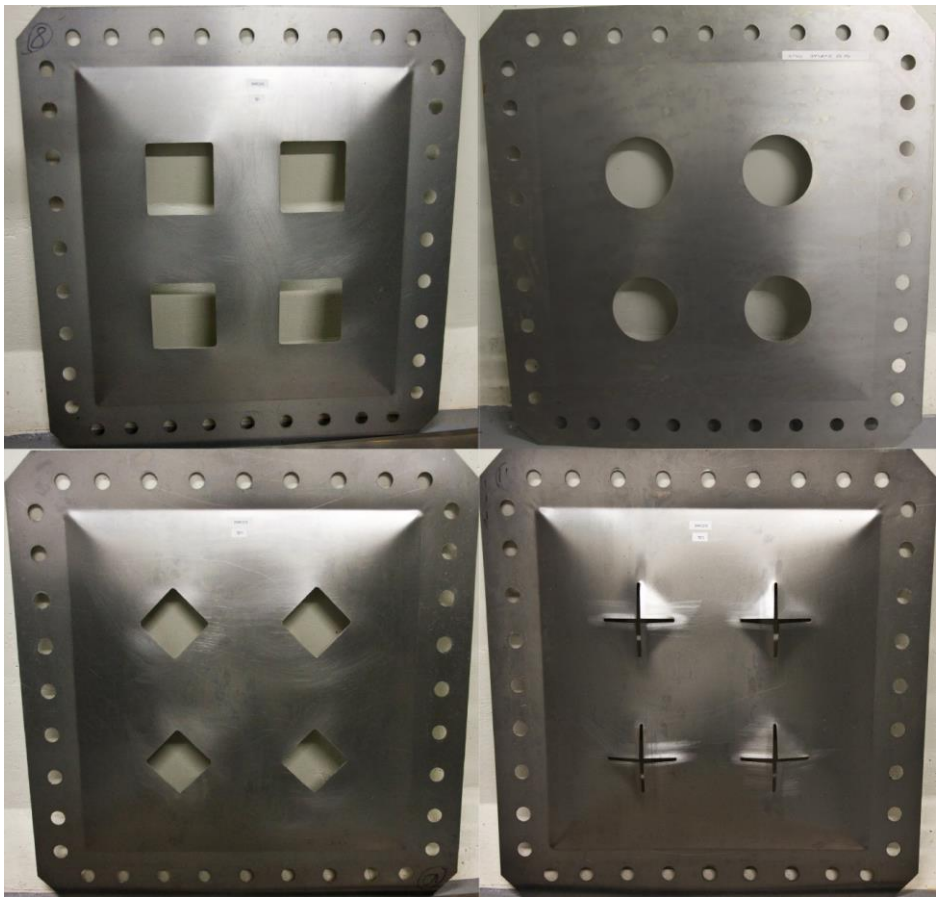

Figure 10: Deformed shapes of the plates exposed to 25 psi nominal pressure.

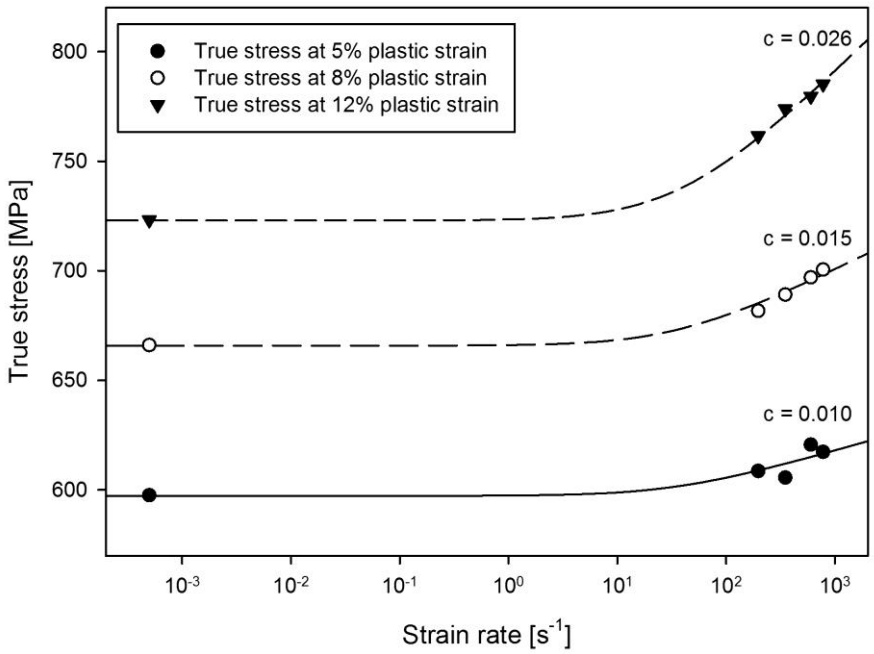

Figure 11: Flow stress as function of strain rate. Experimental data points are shown as dots and the results obtained with the modified Johnson-Cook model, using different values of c for the three levels of plastic strain, are shown as lines.

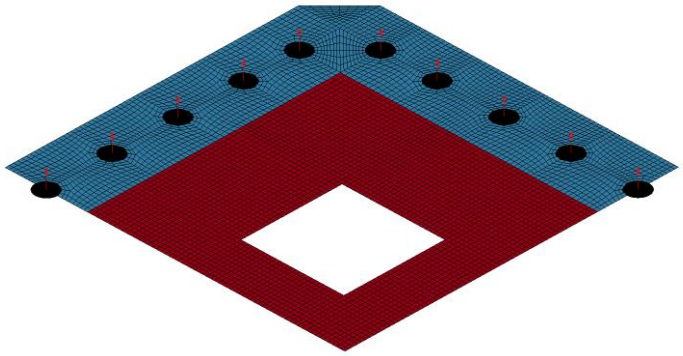

Figure 12: Finite element mesh of a plate with square holes with a characteristic element size of $4 \times 4\,\mathrm{mm}^2$. The bolts are modelled as rigid walls and shown in black. Similar finite element models were generated for the other plate designs.

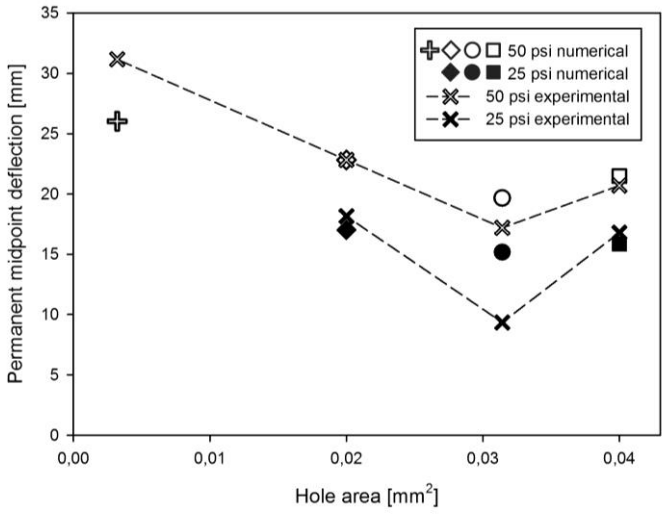

Figure 13: Comparison of permanent midpoint deflections from the experiments and the Lagrangian simulations shown as function of the hole area.

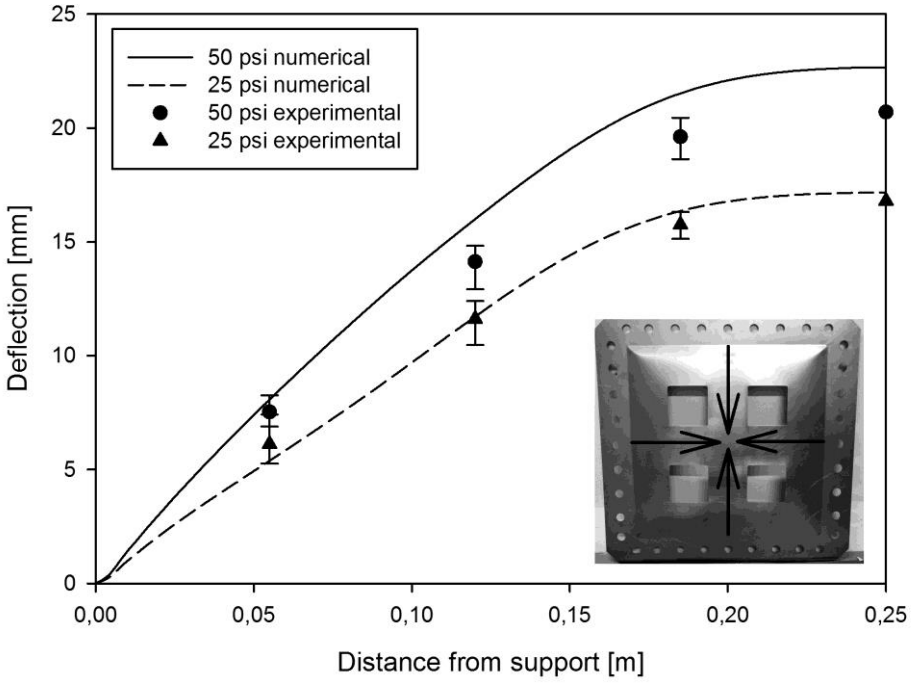

Figure 14: Permanent deflection profile along the directed lines shown in the insert for plates with square holes tested at 25 and 50 psi. Results from the numerical simulations are shown as lines and the experimental data are shown as error bars.

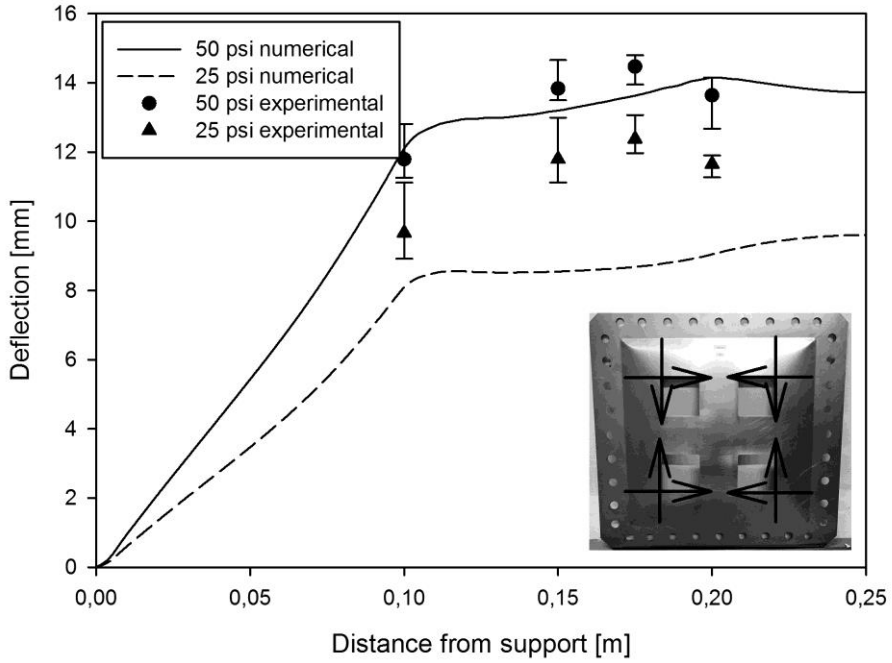

Figure 15: Permanent deflection profile along the directed lines shown in the insert for plates with square holes tested at 25 and 50 psi. Results from the numerical simulations are shown as lines and the experimental data are shown as error bars.

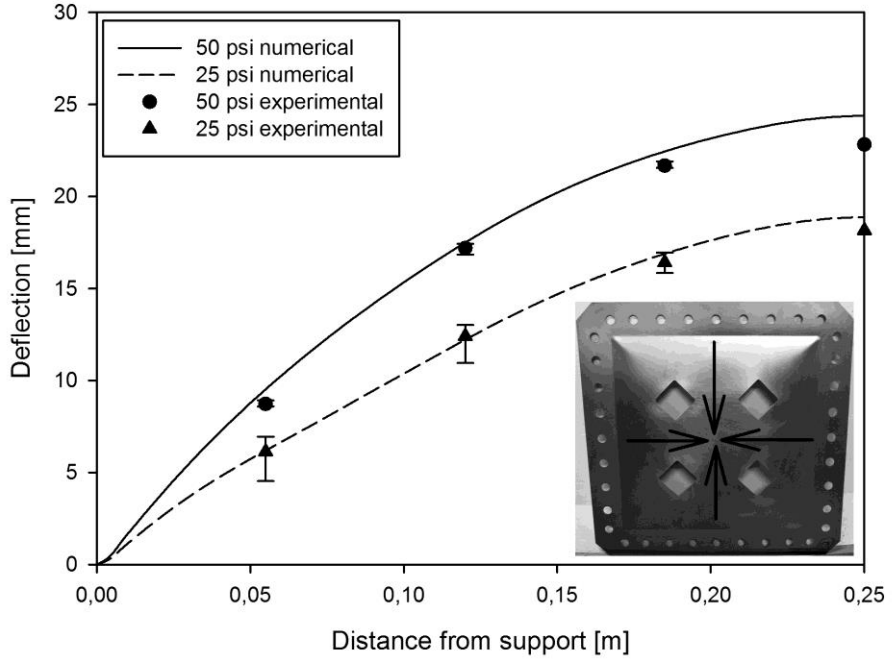

Figure 16: Permanent deflection profile along the directed lines shown in the insert for plates with diamond holes tested at 25 and 50 psi. Results from the numerical simulations are shown as lines and the experimental data are shown as error bars.

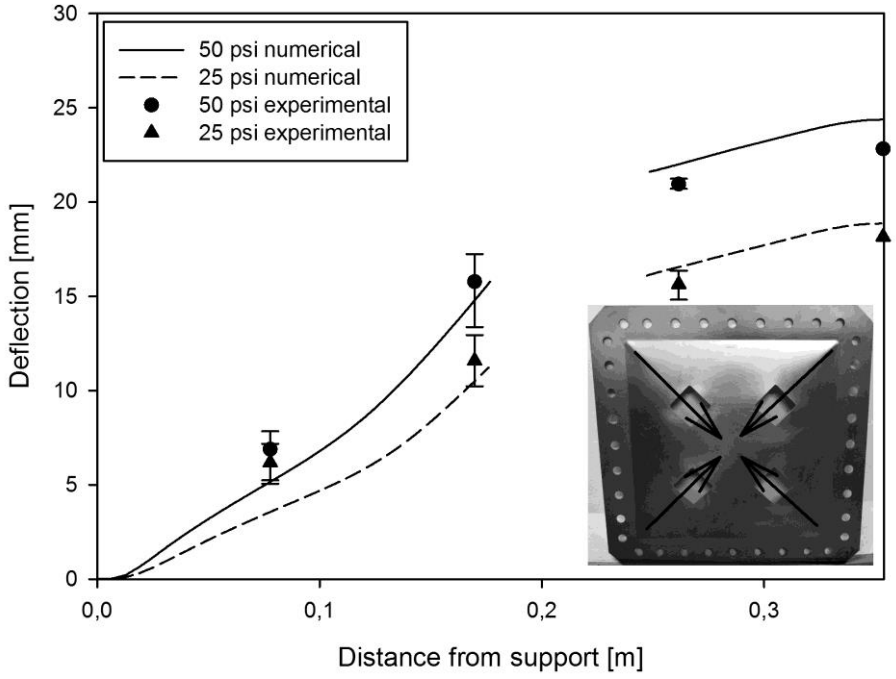

Figure 17: Permanent deflection profile along the directed lines shown in the insert for plates with diamond holes tested at 25 and 50 psi. Results from the numerical simulations are shown as lines and the experimental data are shown as error bars.

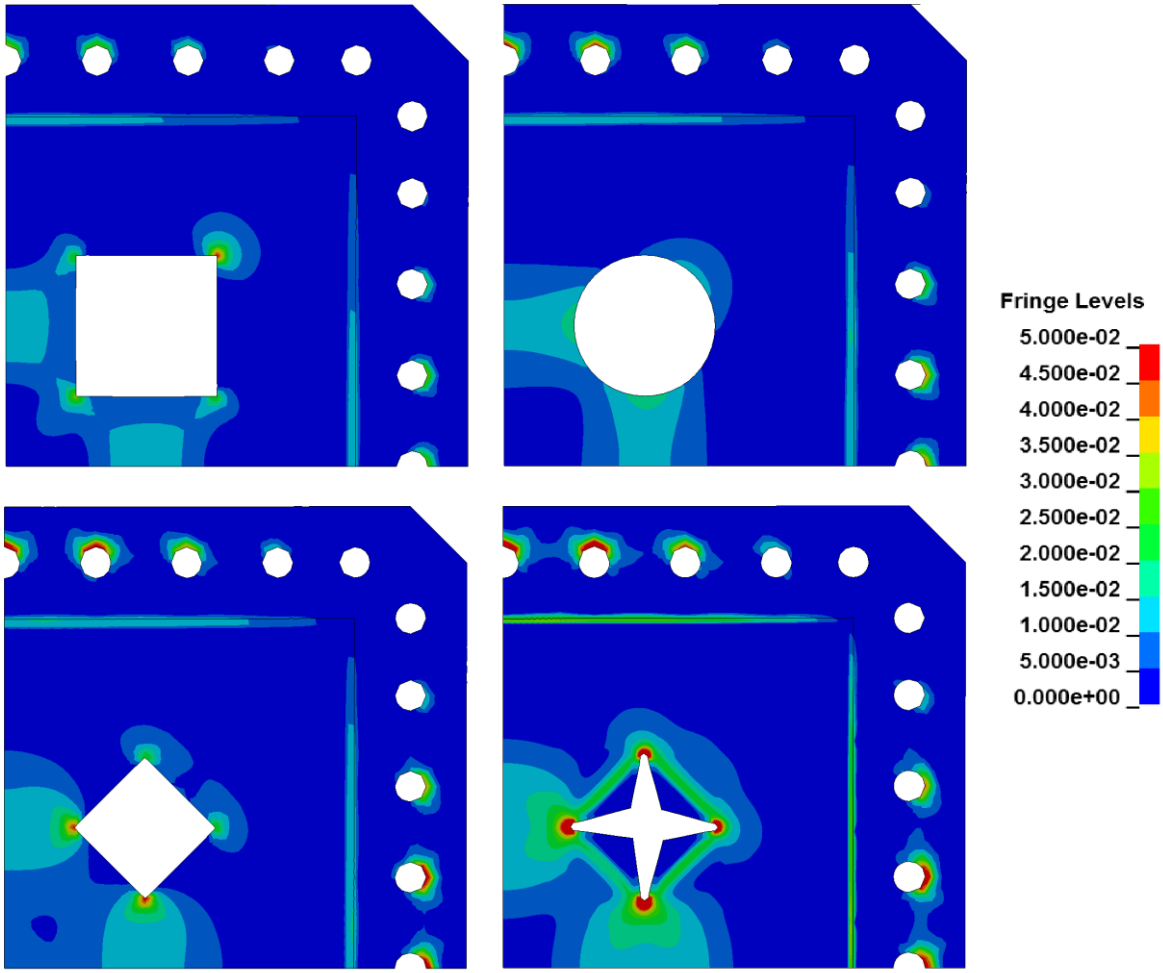

Figure 18: Fringes of equivalent plastic strain plotted on the deformed shapes close to the holes of the various plate designs after 50 psi nominal pressure loading.

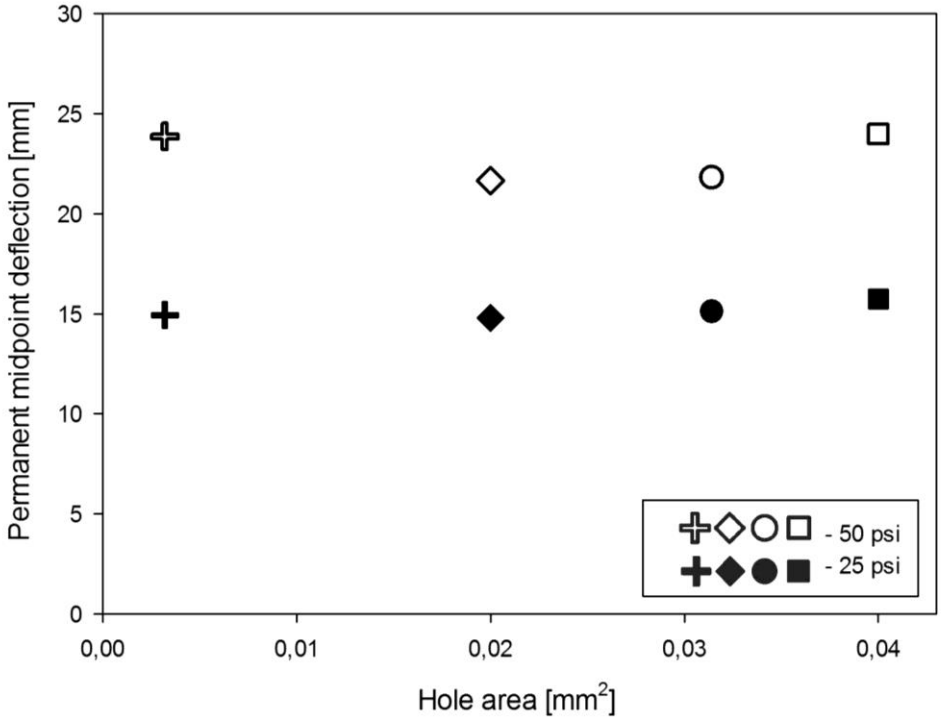

Figure 19: Predicted permanent midpoint deflections for the plates assuming the same pressure-time history, but different loading area. Plotted as function of the hole area.

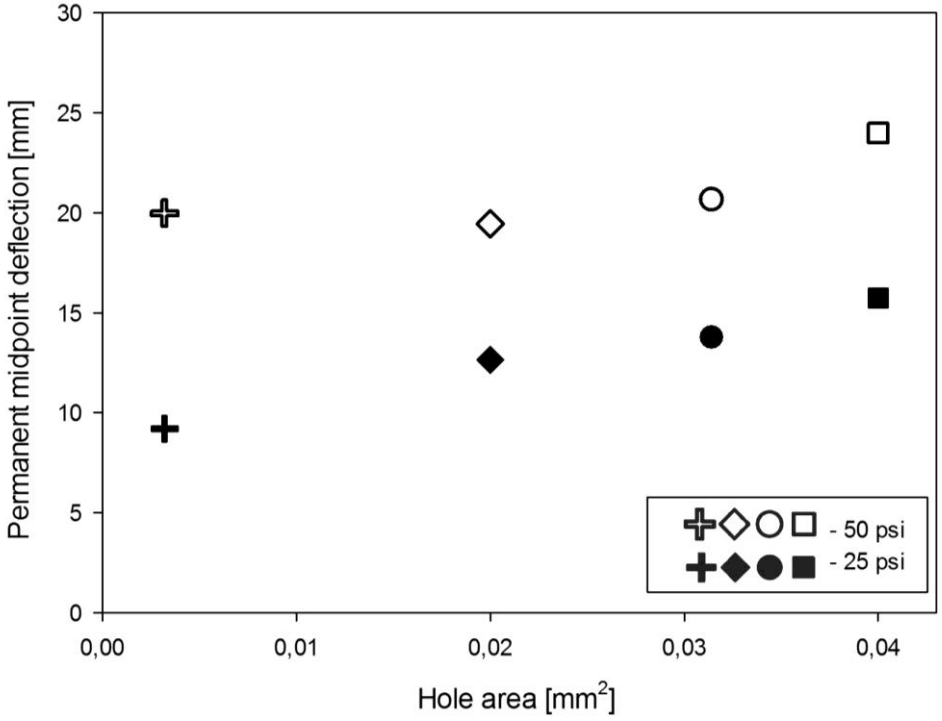

Figure 20: Predicted permanent midpoint deflections for the plates assuming the same pressure-time history and equal loading area. Plotted as a function of the hole area.

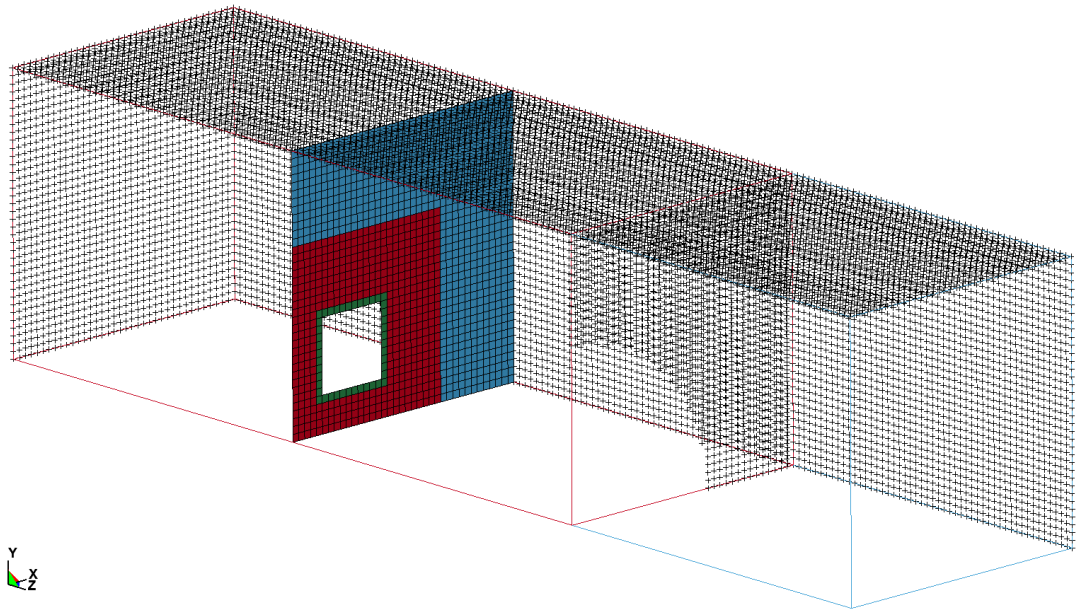

Figure 21: FSI finite element mesh of the 25 psi nominal gauge pressure experiment of a plate with square holes. The fixed boundary conditions for the pressurized air are shown as dark crosses.

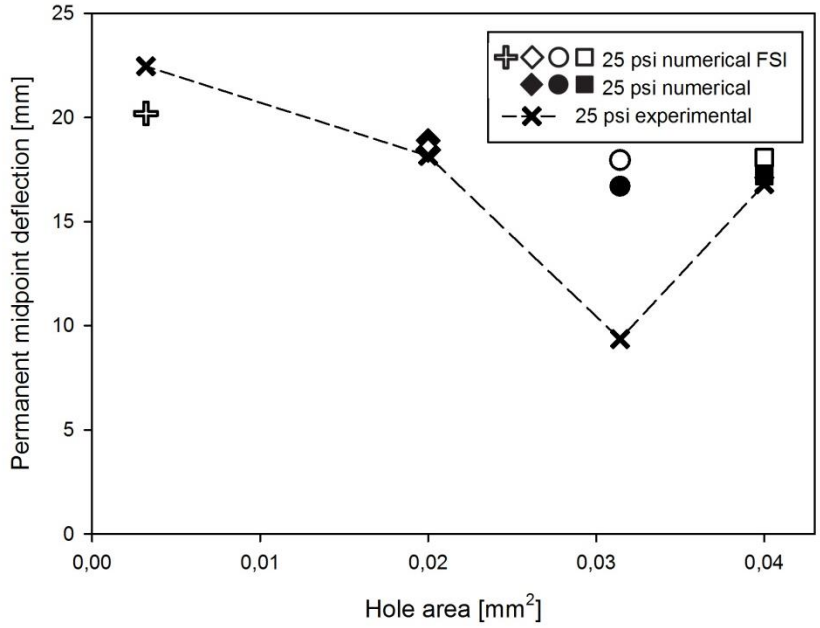

Figure 22: Permanent midpoint displacement from the FSI analyses compared with the experimental and simplified numerical results

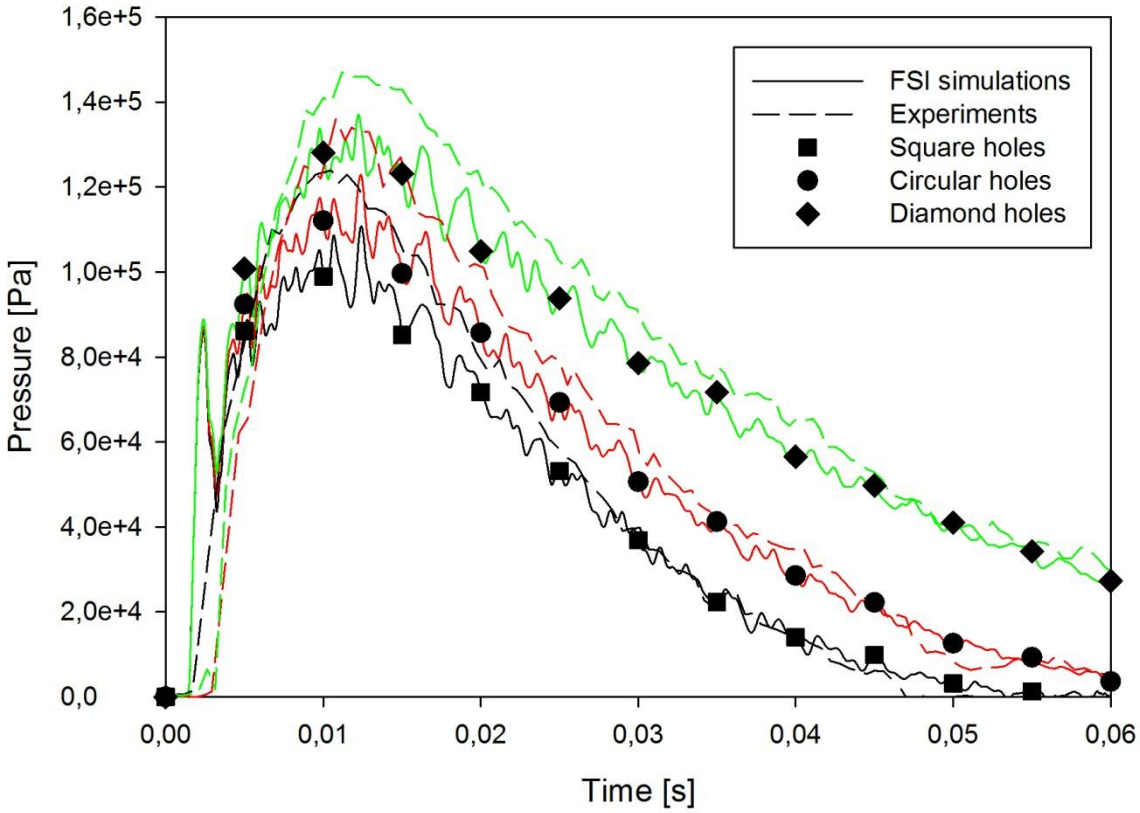

Figure 23: Comparison of recorded pressure-time series from experiments and FSI simulations

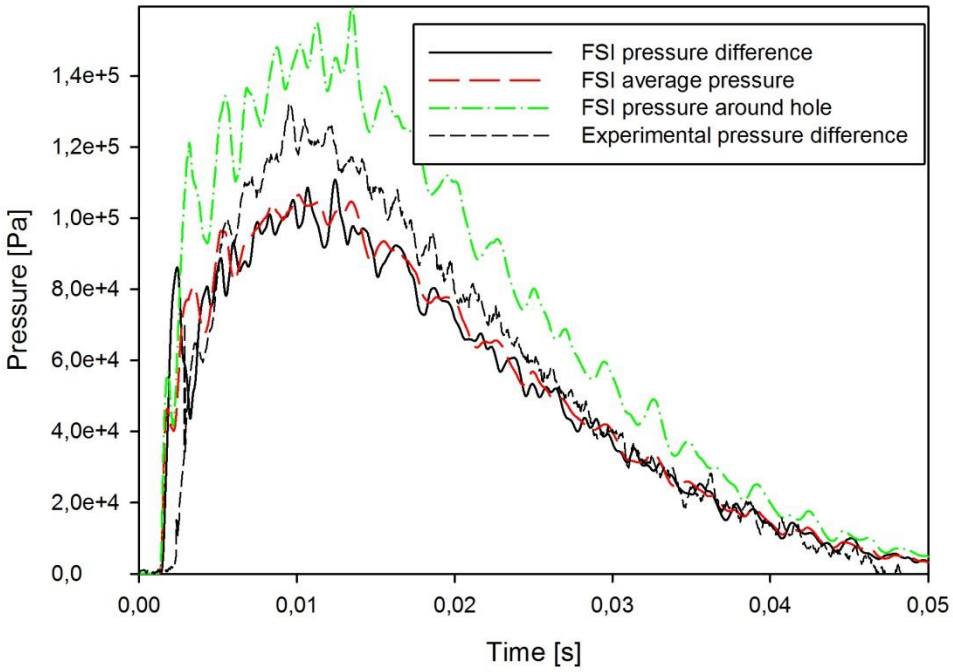

Figure 24: Pressure-time histories from FSI simulations of the 25 psi nominal pressure test of a plate with square holes compared with the measured results.

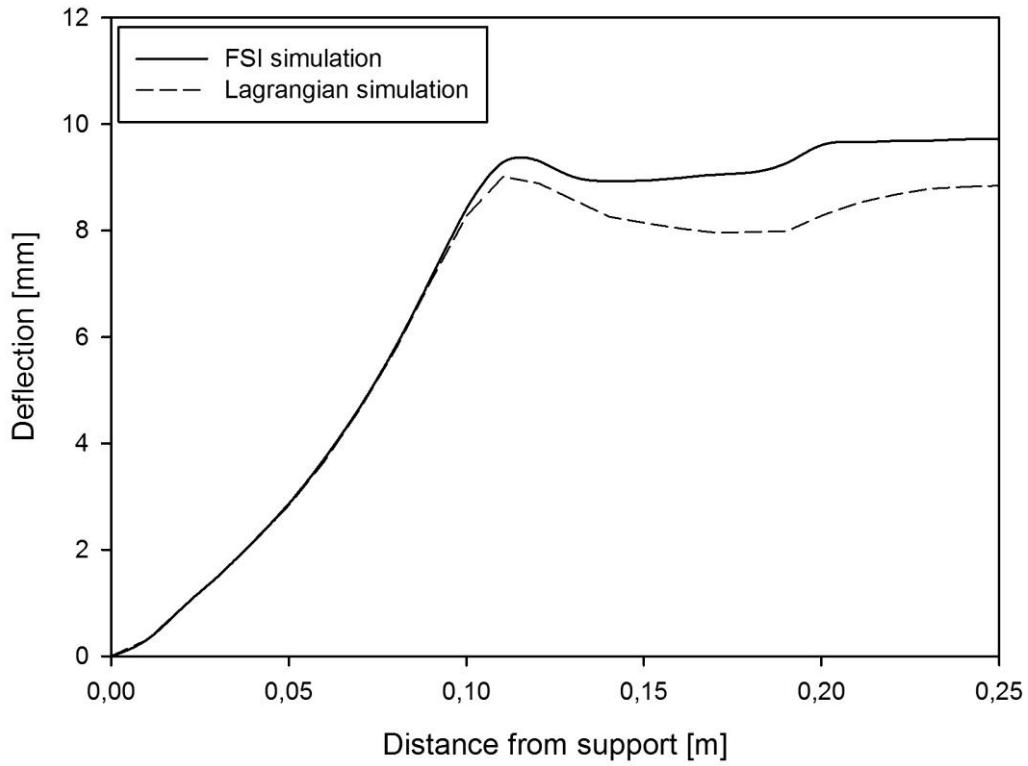

Figure 25: Permanent deflection profile along the same directed lines as in Figures 14 and 15 for a plate with square holes simulated both with FSI and an equivalent pressure load without spatial variation in a Lagrangian simulation.